Science Advances
AAAS

advances.sciencemag.org/cgi/content/full/4/7/eaat3151/DC1

Supplementary Materials for

Adsorbate-driven reactive interfacial Pt-NiO_{1-x} nanostructure formation on the $Pt_3Ni(111)$ alloy surface

Jeongjin Kim, Woong Hyeon Park, Won Hui Doh, Si Woo Lee, Myung Cheol Noh, Jean-Jacques Gallet, Fabrice Bournel, Hiroshi Kondoh, Kazuhiko Mase, Yousung Jung*, Bongjin Simon Mun*, Jeong Young Park*

*Corresponding author. Email: ysjn@kaist.ac.kr (Y.J.); bsmun@gist.ac.kr (B.S.M.); jeongypark@kaist.ac.kr (J.Y.P.)

Published 13 July 2018, *Sci. Adv.* **4**, eaat3151 (2018)
DOI: 10.1126/sciadv.aat3151

The PDF file includes:

Other Supplementary Material for this manuscript includes the following:

(available at advances.sciencemag.org/cgi/content/full/4/7/eaat3151/DC1)

Movie S1 (.avi format). Time-lapse AP-STM movie on the $Pt_3Ni(111)$ surface under mixed CO/O_2 (1:5 ratio) gas at 300 K.

Supplementary Text

Bimetallic Pt-Ni surface on $Pt_3Ni(111)$ single crystal

The 'worm-like' surface structures of $Pt_3Ni(111)$ are one of the characteristic features of bimetallic materials that are created by elemental dislocations along the surface boundaries. The Pt-Ni alloy material has lattice constants of 3.91 Å (Pt) and 3.35 Å (Ni) with an *fcc*-structure for both. The bulk structures for both the Pt and Ni have similar crystallographic geometries and they share an optimized lattice constant for the bulk alloy structure (3.88 Å); however, at least three of the atomic layers along the top of the surface have irregular element compositions because of the preparation or handling methods for the alloyed materials. Consequently, the lattice mismatch between the Pt and Ni atoms is the dominant driving force that continuously leads to the unexpected formation of each domain structure on the $Pt_3Ni(111)$ surface until the disordered Pt-Ni networks reach a stable thermodynamic energy. During this process, a domain element of the alloying network is lifted or lowered to reduce the surface energy at the boundary using the strain effect. These puzzling atomic-level motions that occur on just a few layers of the bimetallic surface are crucial for constructing the unusual electronic structure, which differs from the well-known properties of single-metal or metal oxide materials.

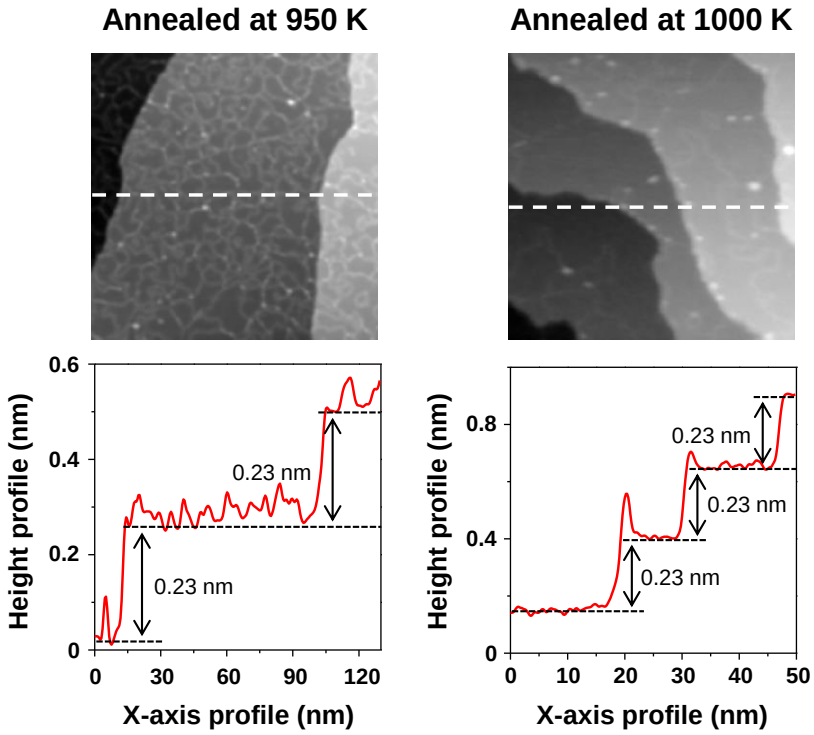

Fig. S1. Formation of the bimetallic domain structures. (top) STM images showing the random Pt-Ni domain structures on the $Pt_3Ni(111)$ surface at UHV and 300 K where the samples were annealed at (left) 950 K [V_s = 1.25 V; I_t = 0.26 nA] and at (right) 1000 K [V_s = 1.25 V; I_t = 0.21 nA]. The faint lines at the domain boundaries on the terrace sites of the pristine $Pt_3Ni(111)$ surface disappear as a function of annealing temperature in UHV. Both STM images show a clear step-terrace structure consisting of the same monoatomic step heights as Pt(111), as shown in the representative line profiles (bottom).

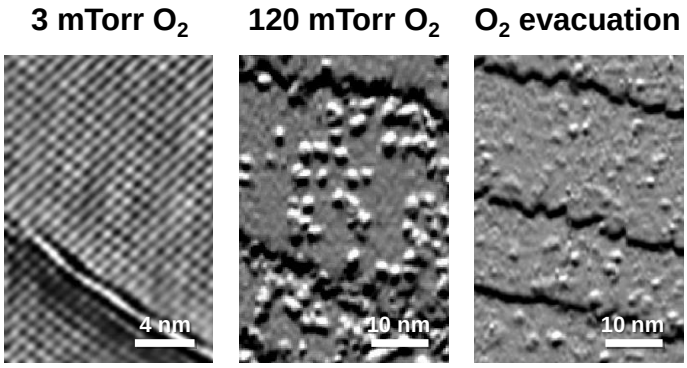

Fig. S2. Oxygen-induced surface restructuring. Z-axis differentiated AP-STM images of the oxygen-induced $Pt_3Ni(111)$ surface at 300 K and 3 mTorr of O_2 [V_s = 1.25 V; I_t = 0.200 nA], 120 mTorr of O_2 [V_s = 1.40 V; I_t = 0.280 nA], and O_2 evacuation [V_s = 1.25 V; I_t = 0.160 nA]. The dissociated oxygen is adsorbed on the topmost Pt-skin layer of the $Pt_3Ni(111)$. At 3 mTorr of O_2, a chemisorbed $p(2 \times 2)$-O structure forms on the surface. At 120 mTorr of O_2, segregated Ni oxide clusters are clearly seen on the AP-STM image. The clusters remained on the $Pt_3Ni(111)$ surface after O_2 evacuation.

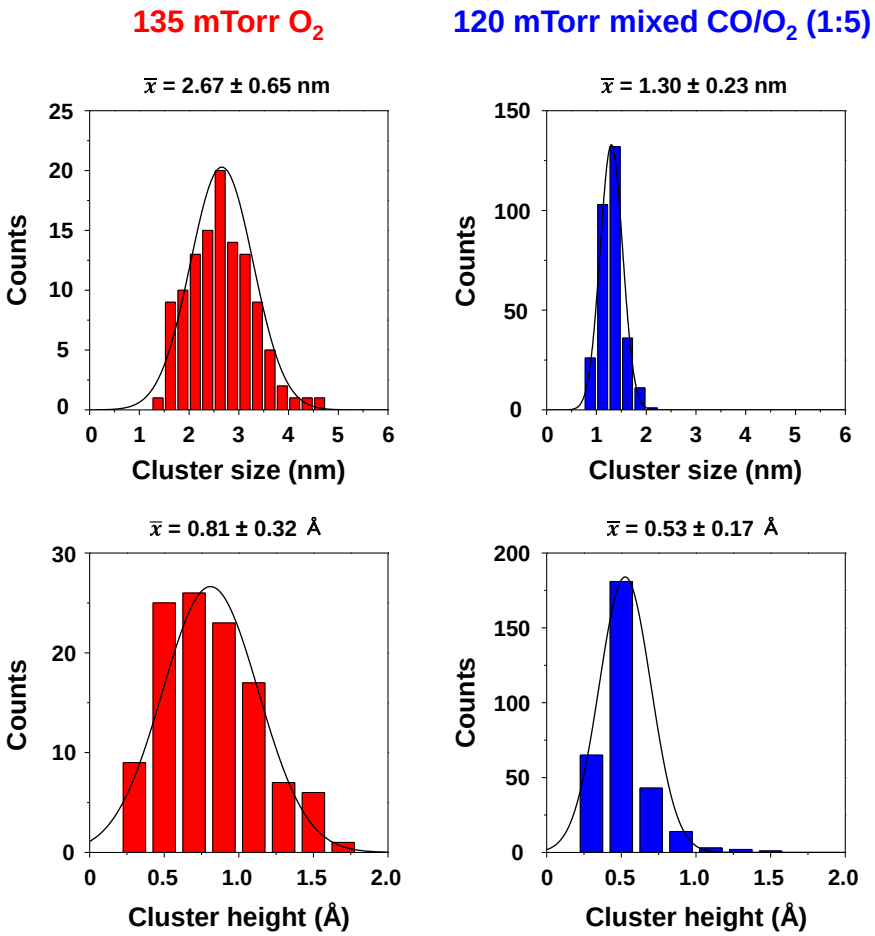

Fig. S3. Statistical analysis plots for NiO_{1-x} clusters. Cluster size and height distributions of the NiO_{1-x} clusters evolved on the $Pt_3Ni(111)$ surface at 300 K under (left) 135 mTorr of O_2 and (right) 120 mTorr of mixed CO/O_2 (1:5 ratio) gas, obtained from STM images.

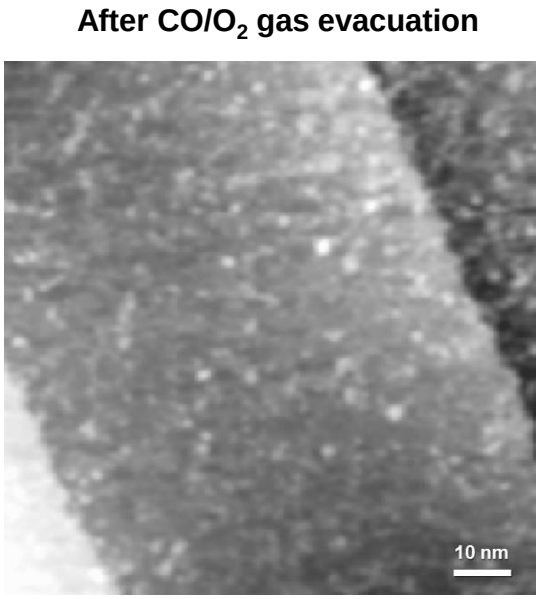

Fig. S4. Direct observation of the $Pt_3Ni(111)$ after CO/O_2 gas evacuation. STM image on the $Pt_3Ni(111)$ surface taken at UHV after the experiment with 120 mTorr of mixed CO/O_2 (1:5) gas [V_s = 1.40 V; I_t = 0.330 nA].

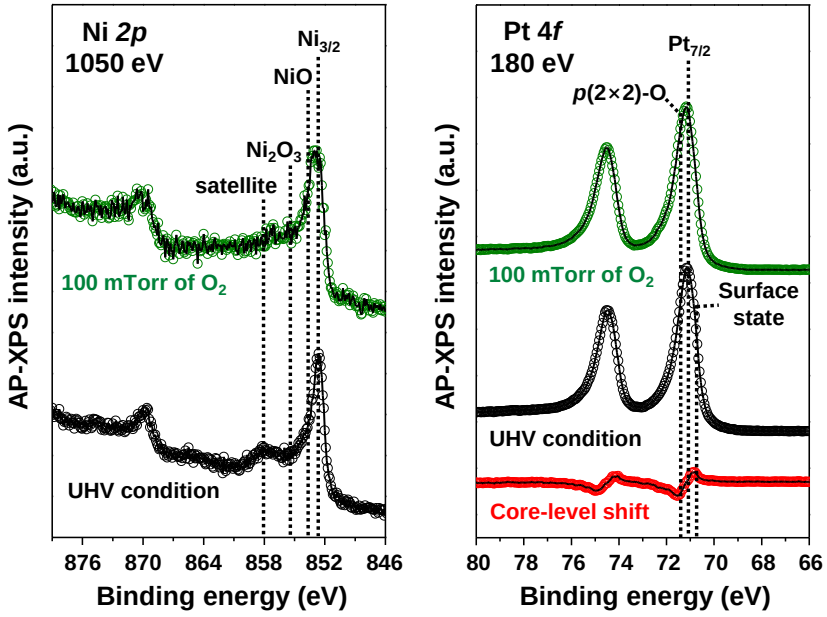

Fig. S5. AP-XPS analysis at 100 mtorr of O_2. AP-XPS core-level spectra for Ni 2*p* (*hv* = 1050 eV) and for Pt 4*f* (*hv* = 180 eV) on the $Pt_3Ni(111)$ surface at 300 K in UHV (black) and 100 mTorr of O_2 (green). The core-level shift for the Pt 4*f* spectra (red) is also plotted to show the detailed spectral changes by spectrum subtraction (UHV condition − 100 mTorr of O_2).

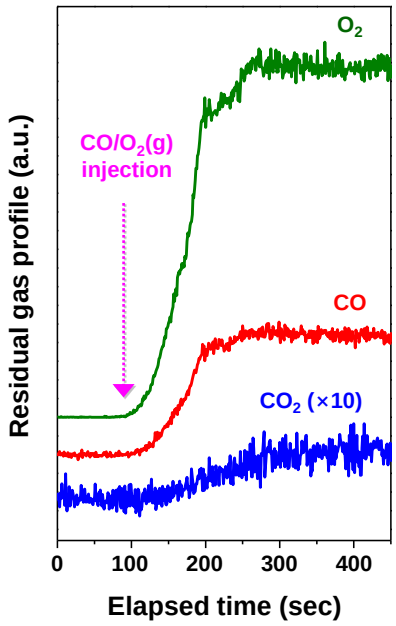

Fig. S6. Tracking the mass profiles at room temperature. Residual gas analysis plot on the $Pt_3Ni(111)$ surface at 100 mTorr of mixed CO/O_2 (1:5) gas at 300 K. The traced mass spectrometry profiles are CO (m/z = 28), O_2 (m/z = 32), and CO_2 (m/z = 44).

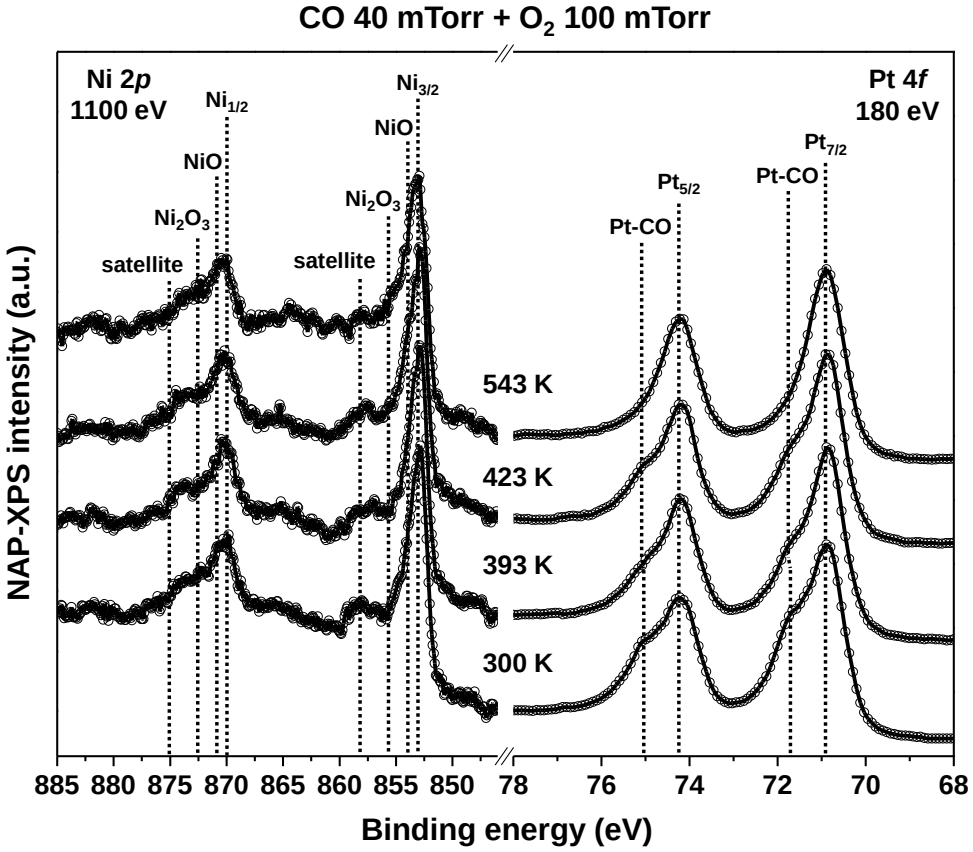

Fig. S7. AP-XPS analysis in mixed CO/O_2 gas at elevated temperature. AP-XPS core-level spectra for Ni 2*p* (*hv* = 1100 eV) and Pt 4*f* (*hv* = 180 eV) on the $Pt_3Ni(111)$ surface under 40 mTorr of CO and 100 mTorr of O_2 mixed gas (1:2.5) at elevated temperatures.

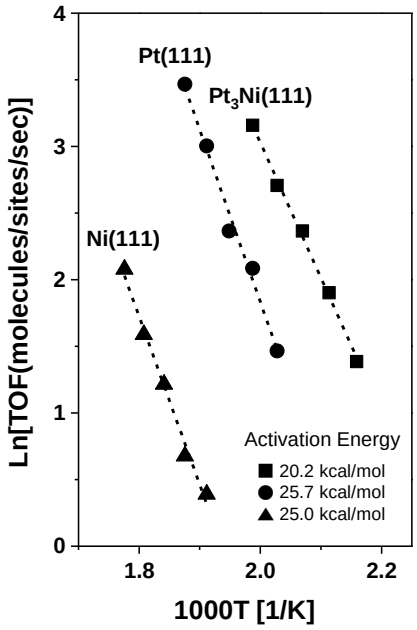

Fig. S8. Arrhenius plots for catalytic activity measurements. Each turnover frequency (TOF) number for $Pt_3Ni(111)$, Pt(111), and Ni(111) was measured under mixed gas (40 Torr CO/100 Torr O_2/620 Torr He) in a batch reactor.

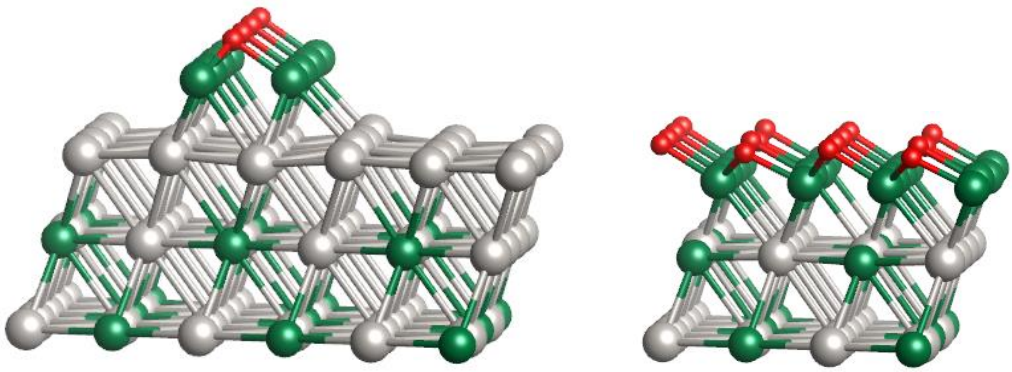

Fig. S9. Model structures of the interfacial Pt-NiO_{1-x} and NiO/Pt_3Ni. DFT calculation models for CO oxidation over (left) the interfacial Pt-NiO_{1-x} and (right) NiO on the stoichiometric Pt_3Ni structure. The colors of each atom in the model are Pt (light-gray), Ni (green), and O (red).

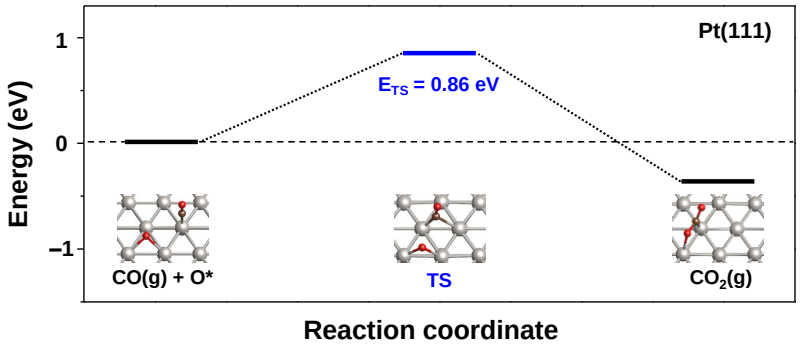

Fig. S10. Energy profile for CO oxidation on the Pt(111). DFT calculation results for the chemical reaction pathway for CO oxidation on the Pt(111) surface. The optimized minimum and transition state (TS) structures are shown in black and blue, respectively. The adsorbed species are denoted with asterisks (*). The colors of each atom in the model are Pt (light-grey), O (red), and C (brown).

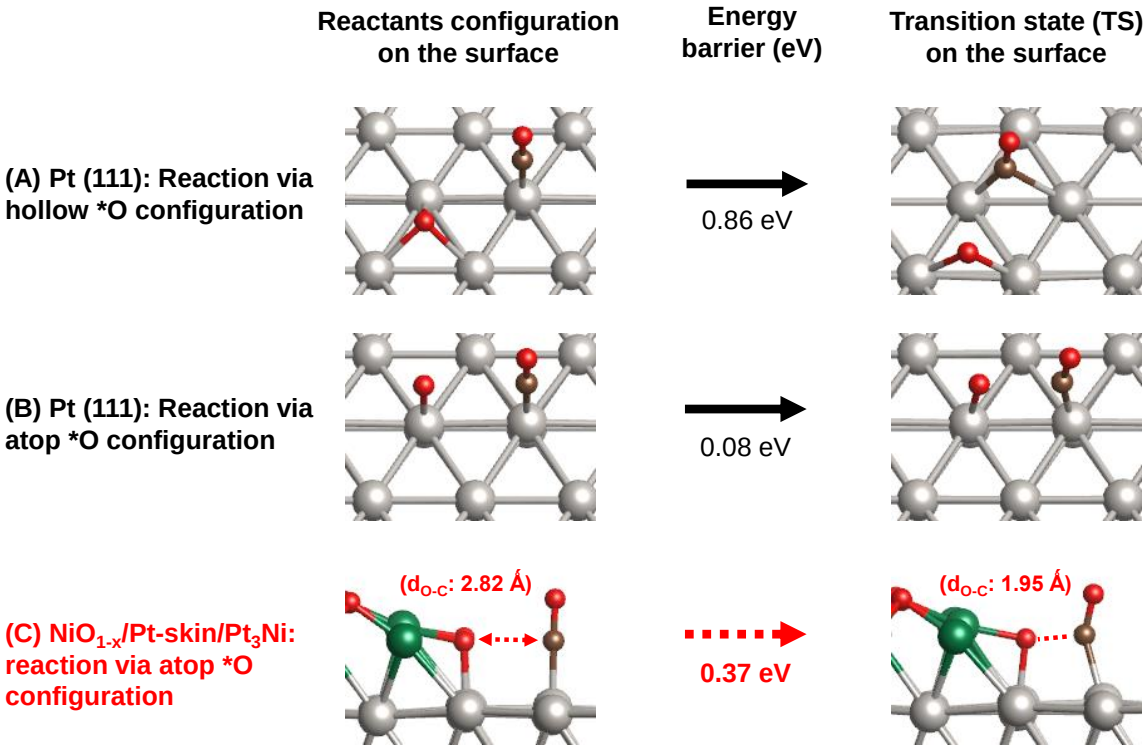

Fig. S11. Activation barriers for the CO oxidation reaction (CO* + O* → CO_2) for different O* configurations on the model surfaces. (**A**) Lowest-energy hollow O* configuration on the Pt(111) surface, (**B**) atop O* configuration (local minimum) on the Pt(111) surface, and (**C**) atop O* configuration at the NiO_{1-x}/Pt-skin/Pt_3Ni interface. When O* is at the atop site, as in (**B**) and (**C**), the O*-metal and CO*-metal bonds undergo less rearrangement/rupture during the reaction to reach TS (the early transition state) with a reduced reaction barrier.

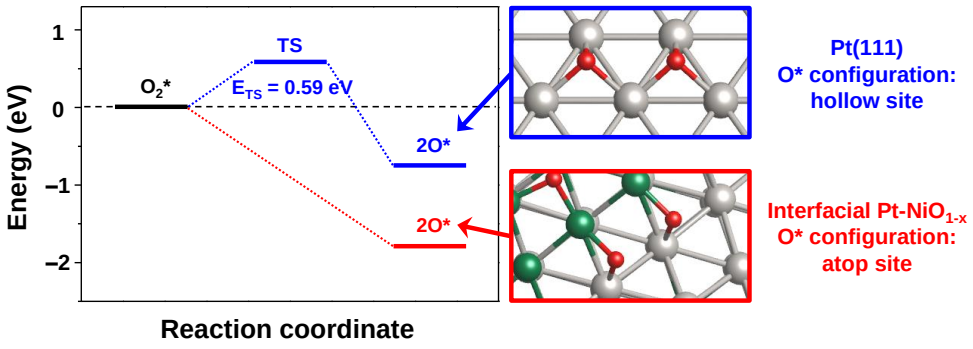

Fig. S12. Energy profile for O_2 dissociation on the Pt(111) surface and on the interfacial Pt-NiO_{1-x} nanostructure. Each optimized structure for dissociated oxygen (O*) adsorption on Pt(111) and the interfacial Pt-NiO_{1-x} nanostructure is shown as an atomistic model (right panel, top and bottom, respectively).

Movie S1. Time-lapse AP-STM movie on the $Pt_3Ni(111)$ surface under mixed CO/O_2 (1:5 ratio) gas at 300 K.